CHEMICAL ENGINEERING TRANSACTIONS
VOL. 84, 2021
A publication of AIDIC
The Italian Association of Chemical Engineering
Online at www.cetjournal.it
Guest Editors: Paolo Ciambelli, Luca Di Palma

ISBN 978-88-95608-82-2; **ISSN** 2283-9216
DOI: 10.3303/CET2184040

Multiphoton Fabrication of Flexible Photo-thermally Active Proteinaceous Microstructures

Amirbahador Zeynali[a,*], Mario Marini[a], Maddalena Collini[a], Margaux Bouzin[a], Laura Sironi[a], Laura D'Alfonso[a], Piersandro Pallavicini[b], Giuseppe Chirico[a,*]

[a] Dipartimento di Fisica, Piazza della Scienza 3, 20126, Milano (I)
[b] Dipartimento di Chimica, Via Taramelli 12, 27100 Pavia
giuseppe.chirico@unimib.it

Two-photon and single photon laser writing are used here to fabricate 3D proteinaceous microstructures with photothermal functionality in the near-infrared spectral region and tunable elasticity. The photo-cross-linking is initiated in bovine serum albumin (BSA) by Rose Bengal and the photo-thermal effect arises from gold nanostars dispersed in the ink. Massive energy transfer of the plasmonic resonances of the gold nanostars to the photo-initiator is avoided by employing an anionic photo-initiator, allowing to obtain effective photo-crosslinking of BSA and to retrieve a substantial photo-thermal efficiency of the fabricated structures. On these microstructures, with a gold atom concentration as low as 1% w/w, a highly localized temperature increase can be quickly (≅1 s) reached and maintained under continuous wave laser irradiation at 800 nm. The photothermal efficiency under continuous wave laser irradiation depends on the thickness of the microstructure and can reach 12.2 +/- 0.4 °C/W. The Young modulus of the fabricated structures is estimated from the measurement of their bending under steady flow and falls in the range of most typical tissues, suggesting that they can be adopted as promising platform for future applications in regenerative nanomedicine.

1. Introduction

Advanced Additive Optical Manufacturing (AOM) allows to fabricate complex micron-size structures with large impact on various fields, from optics to electronics, form biomedicine to tissue engineering. OAM techniques encompass Selective Laser Melting (SLM), Fused Deposition Modeling (FDM), Direct Laser Writing (DLW), Stereolithography (SLA), Direct Inkjet Writing (DIW), inkjet printing, Laser induced Forward Transfer (LIFT), and microcontact printing, to cite a few. They differ for the source, layer-to-layer transfer method and the 3D-writing capability. Non-linear excitation methods has recently fostered the field of laser printing allowing the all-optical 3D writing capability that SLA was lacking of. Maria Göppert-Mayer in 1930 theoretically analysed the possibility of two-photon absorption (TPA), opening the way to its first experimental observations in 1961 (Kaiser et al. 1961) and followed, some thirty years after the first TPA-based polymerization (TPP) experiments (Maruo et al. 1997), by the fabrication of sub-diffraction microstructures (Kawata et al. 2001) with features size ≅ 120nm. Non-linear excitation photo-cross-linking reaches high reaction rates under ambient conditions with relatively low energy input (doses ≅ $3-5\ mJoule$) in aqueous solutions and with limited heat load on the sample. Recently, TPA coupled to STED nanoscopy has led to even finer (≅55nm) writing resolutions (Wollhofen 2013). It is the non-linearity of the TPA effect, with the consequent diffraction limited focal volume, and the use of near Infrared radiation with its ability to penetrate deep into different media (e.g., living-systems), that allowed to reach the three-dimensional resolution both in AOM techniques and in non-linear optical imaging. In multi-photon stereo-lithography the irradiation with a tightly focused and pulsed (≅ 100 fs) laser beam induces the two-photon absorption of the photo-resist in a femtoliter size voxel where it solidifies, due to photochemical processes. By computer aided manufacturing and nano-positioning of either the beam or the stage, one can fabricate arbitrary micro-structures. The careful choice of the photo-resist and the laser source allows to minimize those chemico-physical processes, like local heating or redox reactions,

Paper Received: 24 June 2020; Revised: 24 November 2020; Accepted: 7 February 2021
Please cite this article as: Zeynali A., Marini M., Collini M., Bouzin M., Sironi L., D'Alfonso L., Pallavicini P., Chirico G., 2021, Multiphoton Fabrication of Flexible Photo-thermally Active Proteinaceous Microstructures, Chemical Engineering Transactions, 84, 235-240 DOI:10.3303/CET2184040

that limit the minimum size of the microstructure.The 3D-printing methods had from the beginning a huge impact on micro-optics and electronics and allowed the fabrication of electro-optical components for higher bandwidth transmission and faster data processing, including waveguides (Xinyuan 2010), micro-optical elements and ultra-compact objectives (Gissibl 2016). The multiphoton stereo-lithography technique also led to the fabrication of moveable micro-machines for applications in microscopy and microfluidics (Knoška 2020), like micro-gears (Maruo 2003a), fluidic nozzles and micro-needles (Maruo 2003b). These and similar devices can also mimic features of the extracellular matrix (ECM) and allow to investigate in an unprecedented way living systems in their functional behaviours, like adhesion, migration and differentiation, and to quantify parameters that characterize the cell-cell and cell-ECM interactions (Raimondi 2013). These submicron structures are nowadays wide spread as 3D spatially controllable culturing environment. Polymers and biological-based materials micro-structured by multiphoton stereo-lithography can be also doped, stained and functionalized during and after laser writing, allowing sophisticated biological studies like, for example, cancer migration in engineered scaffolds (Tayalia 2008), stem-cell homing (Raimondi et al. 2013), regulation of bacterial growth and development (Otuka 2014) or the engineered contractile tissue model developed by (Christensen et al. 2019).

Despite these successful projects in the biomedical field, still the choice of the photo-resist is the most critical one in the non-linear excitation AOM fabrication for nano-medicine. For non-linear photo-crosslinking the resist is a precursor solution containing a photoinitiator (PI), with high two-photon absorption cross-section in the near infrared spectral region, and a functional monomer. The absorption of light by the PI induces its physical activation and triggers the monomer-monomer cross-linking, often by means of hydrogen extraction. The application of AOM 3D technologies to life science is fostered by the development of new biocompatible photoresists. Commercially available synthetic photo-resists, like OrmoComp, SZ2080, PEGDA, and SU-8, have low cytotoxicity (that arises instead from the photo-initiator molecule), high mechanical strength but limited biodegradability. Focusing on this relevant property, Claeyssen et al. proposed a triblock copolymer containing ε-caprolactone, small PEG chains, and trimethylenecarbonate (Claeyssen 2009), showing that one can reach reasonable cell-proliferation on the fabricated structures and a biodegradation time ≅ 1 month for the micro-structure itself. Terzaki et al., by using a modified resin comprising methacryloxypropyl trimethoxysilane, zirconium propoxide, and (dimethylamino) ethyl methacrylate, studied the mechanical and cell-adhesion properties. The printed structures showed biocompatibility up to 3 days (Terzaki 2013). Käpylä et al., with the purpose to maximize the potential of biomimetic microstrucutres, designed polyaminoacids based on methacryloylated and acryloylated poly[N(5)-(2-hydroxyethyl) l-glutamine] (Käpylä 2014).

On the other hand, proteins like collagen, elastin, and fibronectin have intrinsic biocompatibility and biodegradability and can be used as monomers whose cross-linking occurs through the formation of hydroperoxide (R-O-OH) or organic peroxide (R-O-OR) radicals, typically due to a ring-opening reaction or aromatic amminoacids of cysteine or methionine. The fabricated microstructures are weak hydrogels with large pH-sensitive swelling ratios. By mixing polymers and proteins, one can obtain photo-crosslinked structures with good mechanical stability and the cell affinity (Torgersen 2013). Bovine serum albumin (BSA) is listed among the most employed proteins in the field of AOM because of its well-studied functionalities, low cost, stimuli-responsive, and similarities to the human serum albumin (Wei 2017). Serien et al. explored two-photon crosslinking of BSA using Rose Bengal as photoinitiator and characterized the biocompatibility and the pH-responsiveness of the fabricated 3D microstructures (Serien et al. 2017). Finally, the possibility to endow the proteinaceous micro-structured hydrogels with switchable chemical and physical properties, like photo-thermal (Borzenkov 2020) or piezo-electric (Kim 2014), is promising for future applications in tissue engineering.

The goal of the present contribution is to show that one can use nonlinear and linear excitation of the protein BSA based photo-resists to fabricate proteinaceous micro- ($\cong 10-50\,\mu m$ in linear size) and meso-structures ($\cong 500-1000\,\mu m$ in linear size), can endow them also with photo-thermal functionality by incorporating photo-thermal nanoparticles and still obtain the mechanical stability necessary to fabricate 3D elongated structures.

2. Materials and methods

2.1 Optical setup

The AOM setup is based on a Ti:Sapph femtosecond laser source (pulse width $\tau_P \cong 250fs$) focused by a microscope-objective (Nikon dry objective 60X, WD = 0.3 mm, NA = 0.85, or Olympus, NA = 1.05, 20x, water immersion, 2 mm WD) on the sample that is moved by a 3-axis piezo-driven (Hera P733 coupled to a Pifoc-P725, Physik Instrument, D) stage mounted on an inverted (Nikon TE300) microscope. The piezo system (Zeynali et al. 2020) is analogically driven by an Arduino© shield. The microstructures were visualized by 2 photons excitation microscopy of Rose Bengal ($\lambda_{exc} \cong 800$ nm, $\lambda_{em} = 580 \pm 30\,nm$).

2.2 BSA –Rose Bengal ink and GNS synthesis

50mg/mL bovine serum albumin was dissolved in a Milli-Q water. Rose Bengal (Sigma-Aldrich; dye content 95%) added to the as-prepared protein solution to reach 2mM of concentration. The Gold Nanostars (GNSs; hydrodynamic radius = $26.5 \pm 3\,nm$) were synthesized as described elsewhere (Pallavicini et al. 2013), pegylated (PEG-SH, MW 5000) and diluted in the proteinaceous ink at 35% v/v.

2.3 Thermo-imaging of the irradiated microstructures

The temperature increase was recorded on FLIR E60 thermo-camera (viewing angle = 30 degree with respect to the microscope optical axis at a distance of 40 cm. The samples were dried in an ambient environment right before measurements. A focused ($\cong 30\,\mu m$) and pulsed (100 Hz) He-Ne laser spot was raster scanned on the sample while acquiring thermo-image videos. The temperature profile of each position of the laser spot was fit to a Gaussian and a synthetic image was built as described in (Bouzin et al. 2019).

3. Results and discussion

3.1 Photo-thermally active proteinaceous microstructures

The proteinaceous microstructures doped with GNS nanoparticles can be fabricated once a proper choice of the PI is made. Energy transfer from the GNS to the PI should be carefully avoided in order not to lose the photo-thermal activity of the nanoparticles within the microstructures (Zeynali et al. 2020). The spatial resolution of the TPP writing technique is very high even in the presence of the photo-thermal nanoparticles: one can measure (Figure1A, B) an effective writing resolution of $1.2 \pm 0.1\,\mu m$.
Distinct nanoparticles can be seen in the cyan channel (Figure 1C, λ_{em} = 440 $\pm$ 20 nm) that can be ascribed to GNS luminescence. The analysis of the brightness level of the corresponding spots reveals a multicomponent distribution (Figure 1D) with the largest ($\cong 60\%$) fraction of spots segmented in the TPE fluorescence image corresponding to single nanoparticles. The assignment of the order of aggregation in the under-resolved spots in the cyan channel image can be done from the calibration curve of the signal as a function of the component order, as reported in the Figure 1D (inset). Meso-structures with typical linear size of the order of 100 $\mu m - 1000\,\mu m$, can be fabricated by exploiting single photon absorption of Rose Bengal at 514 nm (Figure 1F).

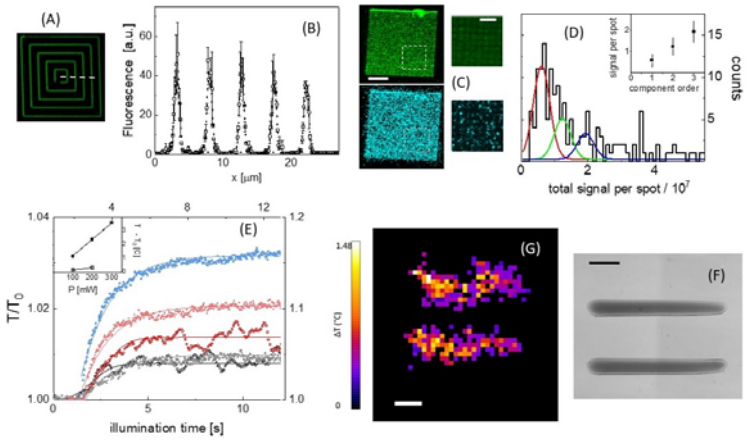

Figure 1. Panel A: maze-like microstructure $50\,\mu m \times 50\,\mu m$ in size written by TPP in the proteinaceous ink doped with GNS nanoparticles. Two-photon fluorescence microscopy image (green channel: λ_{em} =535 $\pm$ 20 nm; Cyan channel: λ_{em} =440 $\pm$ 20 nm). Panel (B): profile along the white dashed line in panel (A) with a multi-components Gaussian fit (dashed line). Panel (C): uniform parallelepiped (scale bar = 15 μm) and zoom-in (scale bar = 5 μm). Panel (D): brightness histogram of individual spots with a three-components Gaussian fit. Inset: average signal per component as a function of the component order. Panel (E): photothermal effect from $20 \times 20 \times 3\,\mu m^3$ proteinaceous uniform microstructures under continuous irradiation (NIR pulsed laser tuned at 800 nm; open symbols, P=100 mW black circles, 200 mW red squares) and meso-structures (filled symbols, P=100 mW, squares; P=200 mW, diamonds; P= 300 mW, triangles) together with single exponential growths (solid lines). Panel G: high resolution thermo-image of a meso-structure (line length = 1420 μm) containing GNS (transmission image in Panel F). Scale bars in panel F and G are 300 μm. Error bars refer to standard deviations computed on triplicates.

Both from these meso-structures and from the microstructures (Figure 1C), one can retrieve a significant photo-thermal effect. The irradiation of the fabricated GNS-doped microstructures with a focused and pulsed laser source tuned at 800 nm produces a rapid increase of the temperature that can be detected by a thermo-

camera and fit to a single exponential growth (solid lines in Figure 1E) with very similar raising time and a value of the plateau temperature (T_∞) that increases linearly with the average power (inset in Figure 1E). The efficiency of the photothermal effect that one obtains from the microstructures, $\frac{\partial(T_\infty - T_0)}{\partial <P>}$ = 1.7 $\pm$ 0.2 $^0C/W$ raises to $\frac{\partial(T_\infty - T_0)}{\partial <P>}$ = 12.2 $\pm$ 0.4 $^0C/W$ for the mesostructures, mainly due to the increase of the active volume thickness that passes from 3-4 μm to about 100 μm. However, the thermal load induced in the meso-structures is less uniform than in the micro-structures, as shown by the high resolution photo-thermal image in Figure 1G, indicating a lower control in the dispersion of the nanoparticles in the meso-structure, compared to the case of the micro-structures (see for comparison Figures 1C and 1G). It is noteworthy that the choice of an anionic PI is essential to preserve the photo-thermal efficiency of the nanoparticles embedded in the proteinaceous hydrogels (Zeynali et al .2020).

3.2 Elongated hollow micro-structures

The Young moduli (E) of the proteinaceous microstructures lies in the range 800 - 1000 kPa depending on the protein/PI ratio: lower values of the protein/PI ratio produce stiffer hydrogels (Zeynali et al. 2020). Even for ratios $\cong 3$, for which E $\cong$ 800 kPa is expected, one can indeed produce less stiff structures by playing with the structure cross-section. An example is given in Figure 2 where hollow tubes of square cross-sections are visualized by fluorescence confocal microscopy of the residual Rose Bengal.

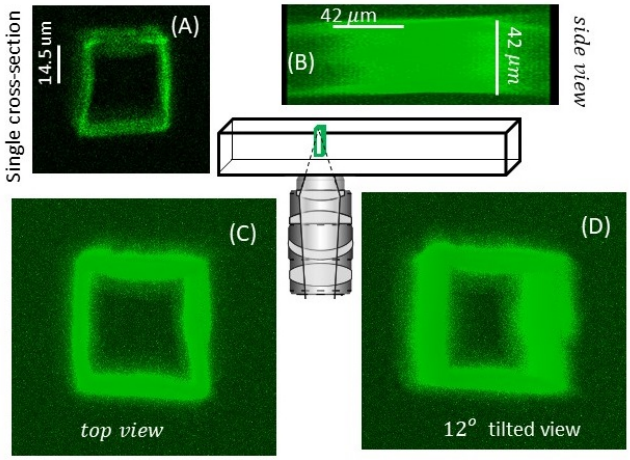

Figure 2. Confocal fluorescence images of hollow microstructures fabricated in BSA – Rose Bengal inks. Panel A: single cross-section. Panel B: side view of the microstructure. Panel C and D: top view snapshots of the 3D reconstruction of the tubular microstructure. Sketch: top-down TPP writing configuration of a square section micro-capillary (100 μm in size).

In order to fabricate such elongated structures, the resist was polymerized hanging from the ceiling of a square section micro-capillary (side length= 100 μm) in a top-down TPP writing protocol. In this way we could avoid the refraction of the laser beam by the written micro-structure and reach high spatial writing resolution throughout the whole optical axis. The square cross-section tubular filament (side $\cong 42\ \mu m$, length $\cong$100 μm; Figure 2A and 2B), is almost perfectly perpendicular to the support glass slide (Figure 2C and Figure 2D).

3.3 Elongated flexible solid meso-structures

Elongated structures have a well-defined bending elasticity. To illustrate this possibility, a meso-structured was fabricated via single-photon excitation of the BSA-RB ink across the section of a square cross-section capillary 300 μm wide (Figure 3A). The section of the structure was thinner at the free end compared to the base, polymerized on the wall of the glass capillary. The base, height and angle are 100 $\mu m, 300\ \mu m, \alpha = 14^0$ (see Figure 3A): the structure is hanging from the top glass wall in Figure 3A and the 100 μm of the structure closer to the wall cannot appreciably move. The stiffness of the structure was probed by flowing water in the capillary at constant rate $\frac{dQ}{dt} \cong 30\ \frac{\mu L}{min}$, with a flow speed $v \cong$ 5.5 mm/s. By approximating this meso-structure with a rod of length L $\cong 200\ \mu m$ and diameter d $\cong 65\ \mu m$ one can estimate the friction coefficient of the structures as (Tirado et al. 1998) $f_\perp = \frac{4\pi\eta L}{\left(ln\left(\frac{L}{d}\right)+\nu_\perp\right)}$, with $\nu_\perp = 0.839 + 0.185\left(\frac{d}{L}\right)^{-1} + 0.233\left(\frac{d}{L}\right)^{-2}$, finding $f_\perp \cong 1.2 \times 10^{-9}\ N\frac{s}{m}$. The average force on the mobile fraction of the mesostructured is therefore approximately $F_{drag} = f_\perp v \cong 6.6\ nN$. The measured deflection of the tip dx = 43 $\pm$ 5 μm observed under such low viscous force implies a value of the elastic constant $k \cong \frac{F_{drag}}{dx} \cong 0.15 \times 10^{-3}\frac{N}{m}$.

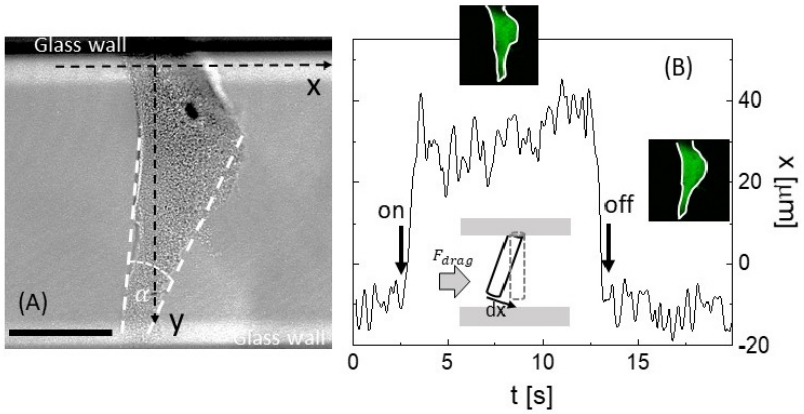

Figure 3. Panel A: proteinaceous meso-structure fabricated across a 300 μm channel (bar= 100 μm) at rest. Panel B: position of the free tip of the mesostructure under constant flow (on at t ≅ 2.6 s and off at t ≅ 13 s).

The Young modulus, Y, of the meso-structure can be estimated from the elastic bending constant of a cylindrical cantilever with diameter section d and length L as (Li 2015) $Y \cong \frac{4L^3k}{d^4}$. Here, one can estimate $Y \cong 270\ kPa$, very similar to the values of the Young moduli of most soft tissues (Akhtar et al. 2011, de Loubens et al. 2014).

4. Conclusions

The data reported here indicate that it is possible to fabricate by laser induced cross-linking of proteins, proteinaceous structures in which photo-thermal nanoparticles are embedded. This is obtained by mixing gold nanostars to proteinaceous photo-resists composed of BSA, the monomer, and Rose Bengal, the photo-initiator. The size of the fabricated structures ranges from $100\mu m$ $(\text{two} - \text{photon excitation})$ to 1mm (single photon excitation) and the photo-thermal efficiency ranges from $\frac{\partial(T_\infty - T_0)}{\partial <P>}$ =11.7 $\pm$ 0.2 $^0C/W$ to $\frac{\partial(T_\infty - T_0)}{\partial <P>}$ = $12.2 \pm 0.4\ ^0C/W$, respectively. This variability is likely due to the different thickness of the structures obtained in the two cases (two and single-photon excitation) that implies a larger number of hot spots in the irradiated volume and, at the same time, an increased volume in which the heat dissipates.
The micro-fabricated proteinaceous hydrogels have a considerable elastic modulus that allows to fabricate elongated hollow tubular structures with cross-section ≅ 100 μm in side. The estimated value of the Young modulus of the structures obtained by single-photon excitation is $Y \cong 270\ kPa$. This observation is particularly relevant for the future application of this kind of structures in the field of microfluidics for biotechnology and of nanomedicine, with particular relevance for tissue engineering. With this purpose, we are currently investigating the effect of highly localized released of heat (< 2 Celsius) on the differentiation of neurons.

Acknowledgments

We acknowledge the support of the University of Milano-Bicocca (ATE-2018 and ATE-2019). G.C. and M.C. also acknowledge the support of the ISASI department of CNR and of INFN.

References

Akhtar R., Sherratt M. J., Cruickshank J. K., Derby B., 2011, Characterizing the elastic properties of tissues, Mater. Today, 14, 96.

Borzenkov M., Chirico G., Pallavicini P., Sperandeo P., Polissi A., Dacarro G., Doveri L., Collini M., Sironi L.; Bouzin M., D'Alfonso L., 2020, Nanocomposite Sprayed Films with Photo-Thermal Properties for Remote Bacteria Eradication, Nanomaterials, 10(4), 786.

Bouzin M., Marini M., Zeynali A., Borzenkov M., Sironi L., D'Alfonso L., Mingozzi F., Granucci F., Pallavicini P., Chirico G., Collini M., 2019, Photo-activated raster scanning thermal imaging at sub-diffraction resolution, Nat. Commun., 10, 5523.

Christensen R. K., Von Halling Laier C., Kiziltay A., Wilson S., Larsen N. B., 2019, 3D printed Hydrogel Multiassay platforms for robust generation of engineered contractile tissues, Biomacromolecules, 21(2), 356-365.

Claeyssens F., Hasan E., Gaidukeviciute A., Achilleos D., Ranella A., Reinhardt C., Ovsianikov A., Shizhou X., Fotakis C., Vamvakaki M., Chichkov B., Farsari M., 2009, Three-Dimensional Biodegradable Structures Fabricated by Two-Photon Polymerization, Langmuir, 25(5), 3219–3223.

de Loubens C., Deschamps J., Georgelin M., Charrier A., Edwards-Levyc F., Leonetti M., 2014, Mechanical characterization of cross-linked serum albumin microcapsules, Soft Matter, 10, 4561.

Gissibl T., Thiele S., Herkommer A., Giessen H., 2016, Two-photon direct laser writing of ultracompact multi-lens objectives, Nature Photonics, *10*(8), 554-560.

Kaiser W., Garrett C. G. B., 1961, Two-Photon Excitation in CaF_2:Eu^{2+}, Phys. Rev. Lett., 7, 229

Käpylä E., Sedlačík T., Aydogan D. B., Viitanen J., Rypáček F., & Kellomäki M. 2014, Direct laser writing of synthetic poly(amino acid) hydrogels and poly(ethylene glycol) diacrylates by two-photon polymerization. Materials Science and Engineering: C, 43, 280-289.

Kawata S., Sun H., Tanaka T., & Takada K., 2001, Finer features for functional microdevices. *Nature*, *412*(6848), 697-698.Kim K., Zhu W., Qu X., Aaronson C., McCall W.R., Chen S.C., Sirbuly D.J., 2014, 3D Optical Printing of Piezoelectric Nanoparticle - Polymer Composite Materials, ACS NANO 8(10): 9799-9806

Knoška, J., Adriano, L., Awel, S., Beyerlein, K. R., Yefanov, O., Oberthuer, D., Peña Murillo, G. E., Roth, N., Sarrou, I., Villanueva-Perez, P., Wiedorn, M. O., Wilde, F., Bajt, S., Chapman, H. N., & Heymann, M., 2020, Ultracompact 3D microfluidics for time-resolved structural biology, Nature Communications, 11(1).

Li R., Ye H., Zhang W., Ma G., Su Y., 2015, An analytic model for accurate spring constant calibration of rectangular atomic force microscope cantilevers, Scientific Reports. 5:15828

Maruo, S., Nakamura, O., & Kawata, S., 1997, Three-dimensional microfabrication with two-photon-absorbed photopolymerization. *Optics Letters*, *22*(2), 132.

Maruo, S., Ikuta, K., and Korogi, H., 2003a, Force-controllable, optically driven micromachines fabricated by single-step two-photon micro stereolithography. *J. Microelectromech. Syst.*, 12, 533–539.

Maruo, S., Ikuta, K., and Korogi, H., 2003b, Submicron manipulation tools driven by light in a liquid. *Appl. Phys. Lett.*, 82, 133–135.

Tirado M. M., C.L Martinez, J Garcia de la Torre, 1984, Comparison of theories for the translational and rotational coefficients of rod-like macromolecules. Application to short DNA fragments. J. Chem. Phys. 81, 2047

Otuka, A., Corrêa, D., Fontana, C., & Mendonça, C., 2014, Direct laser writing by twophoton polymerization as a tool for developing microenvironments for evaluation of bacterial growth. Materials Science and Engineering: C, 35, 185-189.

Pallavicini P., A. Dona, A. Casu, G. Chirico, M. Collini, G. Dacarro, A. Falqui, C. Milanese, L. Sironi, A. Taglietti, 2013, Controlled Synthesis of Gold Nanostars by Using a Zwitterionic Surfactant. Chem. Commun. 49, 6265.

Raimondi, M. T., Eaton, S. M., Laganà, M., Aprile, V., Nava, M. M., Cerullo, G., Osellame, R., 2013, Three-dimensional structural niches engineered via two-photon laser polymerization promote stem cell homing. Acta Biomaterialia, 9(1), 4579-4584.

Serien, D., & Takeuchi, S., 2017, Multi-component Microscaffold with 3D spatially defined proteinaceous environment. ACS Biomaterials Science & Engineering, 3(3), 487-494.

Tayalia, P., Mendonca, C. R., Baldacchini, T., Mooney, D. J., & Mazur, E., 2008, 3D cell migration studies using two-photon engineered polymer scaffolds. Advanced Materials, 20(23), 4494-4498.

Terzaki, K., Kissamitaki, M., Skarmoutsou, A., Fotakis, C., Charitidis, C. A., Farsari, M., Vamvakaki, M., & Chatzinikolaidou, M., 2013, Pre-osteoblastic cell response on threedimensional, organic-inorganic hybrid material scaffolds for bone tissue engineering. Journal of Biomedical Materials Research Part A, 101A(8), 2283-2294.

Torgersen, J., Qin, X., Li, Z., Ovsianikov, A., Liska, R., & Stampfl, J., 2013, Hydrogels for two-photon polymerization: A toolbox for mimicking the Extracellular matrix. Advanced Functional Materials, 23(36), 4542-4554.

Wei, S., Liu, J., Zhao, Y., Zhang, T., Zheng, M., Jin, F., Dong, X., Xing, J., & Duan, X., 2017, Protein-based 3D microstructures with controllable morphology and pH-responsive properties. ACS Applied Materials & Interfaces, 9(48), 42247-42257.

Wollhofen, R., Katzmann, J., Hrelescu, C., Jacak, J., & Klar, T. A., 2013, 120 nm resolution and 55 nm structure size in STED-lithography. *Optics Express*, *21*(9), 10831.

Xinyuan, D., Wang, X., Lin, X., Ding, D., Pan, D., & Chen, R., 2010, Highly flexible polymeric optical waveguide for out-of-plane optical interconnects. *Optics Express*, *18*(15), 16227.

Zeynali, A; Marini, M; Chirico, G; Bouzin, M.; Borzenkov, M.; Sironi, L.; D'Alfonso, L.; Pallavicini, P.; Cassina, V.; Mantegazza, F.; Granucci, F.; Marongiu, L.; Polli, D.; De la Cadena, A.; Collini, M., 2020, Multiphoton Fabrication of Proteinaceous Nanocomposite Microstructures with Photothermal Activity in the Infrared. Adv. Opt. Mat. 2020, 8(13): 2000584